ISSN 1069-3513, Izvestiya, Physics of the Solid Earth, 2020, Vol. 56, No. 6, pp. 749–761. © Pleiades Publishing, Ltd., 2020.
Russian Text © The Author(s), 2020, published in Fizika Zemli, 2020, No. 6, pp. 24–37.

# Recurrence of Deep Long-Period Earthquakes beneath the Klyuchevskoi Volcano Group, Kamchatka

**N. A. Galina[a, b, *], N. M. Shapiro[a, b], D. V. Droznin[c], S. Ya. Droznina[c], S. L. Senyukov[b, c], and D. V. Chebrov[c]**

[a] *Institut des Sciences de la Terre, Université Grenoble Alpes, CNRS, Grenoble, 38400 France*
[b] *Schmidt Institute of Physics of the Earth, Russian Academy of Sciences, Moscow, 123242 Russia*
[c] *Kamchatka Branch, Geophysical Survey, Russian Academy of Sciences, Petropavlovsk-Kamchatskii, 683006 Russia*
**e-mail: nataliya.galina@univ-grenoble-alpes.fr*

Received April 3, 2020; revised June 16, 2020; accepted July 4, 2020

**Abstract**—Long-period earthquakes and tremors, on a par with volcano-tectonic earthquakes, are one of two main classes of volcano-seismic activity. It is believed that long-period volcanic seismicity is associated with pressure fluctuations in the magmatic and hydrothermal systems beneath volcanoes and can therefore be used as a precursor of the impending eruptions. At the same time, the physical mechanism of the long-period seismicity is still not fully understood. In this work, we have studied the long-period earthquakes that occur at the crust–mantle boundary beneath the Klyuchevskoi volcanic group in Kamchatka in order to establish their recurrence law—the relationship between the magnitude and frequency of occurrence of the events. In the region under study, the earthquakes pertaining to this type are most numerous and characterize the state of the deep magma reservoir located at the crust–mantle boundary. The changes in the seismic regime in this part of the magmatic system can be one of the early precursors of eruptions. For a more thorough characterization of the frequency–magnitude relationship of the discussed events, we compiled a new catalog of the deep long-period earthquakes based on the matched-filter processing of continuous seismograms recorded by the network stations of the Kamchatka Branch of the Geophysical Survey of the Russian Academy of Sciences in 2011–2012. For these earthquakes, we also used a magnitude determination method that provides the estimates close to the moment magnitude scale. The analysis of the obtained catalog containing more than 40000 events shows that the frequency–magnitude relationships of the earthquakes markedly deviate from the Gutenberg–Richter power-law distribution, probably testifying to the seismicity mechanism and peculiarities of the sources that differ from the common tectonic earthquakes. It is shown that the magnitude distribution of the deep long-period earthquakes is, rather, described by the distributions with characteristic mean values such as the normal or gamma distribution.

*Keywords:* graph of frequency–magnitude relationship of earthquakes, volcanic seismicity, long-period earthquakes, moment magnitude, statistical analysis

**DOI:** 10.1134/S1069351320060026

## INTRODUCTION

Active processes taking place in volcanoes frequently lead to the generation of seismic waves which are recorded by seismographs in the vicinity of the volcanoes. The recorded seismic signals are one of the main data sources for the deep volcanic processes, and the results of their analysis are vital for monitoring a volcanic activity to detect the signs warning that a volcano prepares to erupt. Seismic activity of volcanoes produces very diverse manifestations in terms of signal characteristics and probable generation mechanisms (Tokarev, 1981; Gordeev, 2007; Chouet and Matoza, 2013). The detailed classifications of volcanic seismicity strongly vary between different countries and even between individual volcanoes; however, seismovolcanic phenomena overall are typically divided into two main groups: (1) long-period (LP) events caused by pressure fluctuations in magmatic and hydrothermal fluids (Chouet, 1996); (2) volcano-tectonic earthquakes reflecting the relaxation of mechanical stresses through strike-slip displacements on microfaults (Roman and Cashman, 2006). The LP seismicity primarily includes LP earthquakes and volcanic tremors. The characteristics of the LP seismicity—intensity, spectral content of signals, recurrence interval (frequency) of the events, source location—provide direct information about the state of magmatic and geothermal fluids which, in turn, largely control eruptive activity. The LP earthquakes differ from moderate tectonic earthquakes in that have a lower frequency range (1–5 Hz) and, in some cases, a harmonic shape of seismic waveforms. These earthquakes are most often

observed in shallow parts of the volcano-magmatic systems (e.g., (Iverson et al., 2006; Neuberg et al., 2006; Bean et al., 2014)) and associated with irregular magma movement through channels, degassing, or interaction of hot magma with hydrothermal fluids (Chouet and Matoza, 2013).

The deep LP (DLP) earthquakes which are typically attributed to the processes taking place in the deep magma reservoirs within the crust–mantle transitional layer are particular interesting (Aki and Koyanagi, 1981; Shaw and Chouet, 1989; White, 1996; Power et al., 2004; Nichols et al., 2011; Aso et al., 2013; Shapiro et al., 2017a; Hensch et al., 2019; Kurihara et al., 2019). DLP seismicity is frequently considered as one of the earliest signs of activation of the magmatic systems forewarning the future eruption and can therefore play an important role in volcano monitoring. However, the physical mechanism generating the DLP earthquake and the relationship between the deep magma transport and seismic radiation remain unclear. The hypotheses of the origin of these earthquakes, inter alia, include thermomechanical stresses associated with cooling of deep intrusions (Aso and Tsai, 2014) or avalanche-like $CO_2$ degassing from the oversaturated basaltic magmas (Melnik et al., 2020). However, the observational data existing to date are insufficient for unambiguous identification of the mechanism of DLP earthquakes.

Based on the statistical analysis of the main parameters of the tectonic earthquakes (magnitude, energy, seismic moment, source size and duration), it is possible to reveal the similarity laws reflecting the physical processes in the sources (e.g., (Kanamori and Anderson, 1975)). Among the main statistical relationships characterizing the physics of seismic sources is the so-called recurrence law which describes how the total number of the occurred earthquakes changes with the magnitude. In the case of the "classical" tectonic earthquakes, this law is expressed by the Gutenberg–Richter frequency–magnitude relationship (Gutenberg and Richter, 1944):

$$\log N = a - bM, \quad (1)$$

where $N$ is the number of earthquakes with magnitude $M$; $a$ is the parameter characterizing seismic activity; and parameter $b$ referred to as the $b$-value is the slope of the frequency–magnitude graph. The $b$-value is very close to 1. This relationship be explained in the context of a scale-invariant model where the earthquakes occur as slips on the fault planes and their probability is inversely proportional to the area of the involved fault segment (e..g., (Stein and Wysession, 2003)). At the same time, the coseismic stress-drop is, on average, independent on the earthquake size (Shaw, 2009).

The results of statistical analysis in volcano seismology are not unequivocal and not as clearly systematized as in the case of the tectonic earthquakes. For example, some authors (Okada et al., 1981; Main, 1987; Lahr et al., 1994, etc.) point out evident deviations of the magnitude distribution of the volcanic LP earthquakes from the Gutenberg–Richter relationship. In other works, the attempts to describe the observations by the Gutenberg–Richter frequency–magnitude distribution lead to the $b$-value determinations substantially larger than 1. These observations show that the mechanisms of the volcanic LP earthquakes are not always fit by the scale-invariant model suitable for the tectonic earthquakes. At the same time, establishing a generally accepted form of the frequency–magnitude relationship for the volcanic LP of earthquakes will require a more detailed analysis of the data recorded from different volcanoes.

In particular, a statistical analysis of the statistical analysis of DLP earthquakes recurrences can contribute to better understanding of a physical mechanism responsible for their generation. One of the world's most intense sources of volcanic DLP earthquakes is located beneath the Klyuchevskoi (Klyuchevskoy) volcano in Kamchatka at the depths of 30–35 km corresponding to the crust– mantle boundary (Gorelchik and Storcheus, 2001; Gorelchik et al., 2004; Shapiro et al., 2017a). Senyukov (2013) studied the dependence of the $b$-value on the depth beneath the Klyuchevskoi volcanic group. The analysis revealed higher $b$-values in the region of a deep magma chamber located at the crust–mantle boundary and generating the DLP earthquake. Gorelchik and Storcheus (2001) suppose that the frequency–magnitude relationship of the earthquakes at these depths is better approximated by a normal distribution. In this paper, we analyze the frequency–magnitude distribution for the Klyuchevskoi DLP earthquakes on a more detailed basis. To this end, we apply a sensitive detection method based on a matched filter and use a magnitude scale based on the estimates of the scalar seismic moment from the records of $S$-waves. The sections below provide a detailed account of the analysis methods and the results of their application to the continuous seismic records for a period of 2011–2012.

## THE KLYUCHEVSKOI VOLCANO GROUP

In this work, we study the Klyuchevskoi volcanic group (KVG) in Kamchatka. KVG is one of the world's largest and most active subduction zone volcanic clusters which comprises 13 closely spaced stratovolcanoes and covers a region with a diameter of ~70 km. The extraordinary volcanic activity of this region is associated with the tectonic setting of KVG (Fig. 1) which is determined by the processes in the junction zone of the Kuril–Kamchatka and Aleutian island arcs (Shapiro et al., 2017b). This region is also host to the subduction of the Hawaiian–Emperor Ridge, and KVG in this framework is located above the edge of the sinking plate.

Thus, the geodynamic models seeking to explain the volcanic activity of this group are complex and incorporate many factors: fluid release from a thick

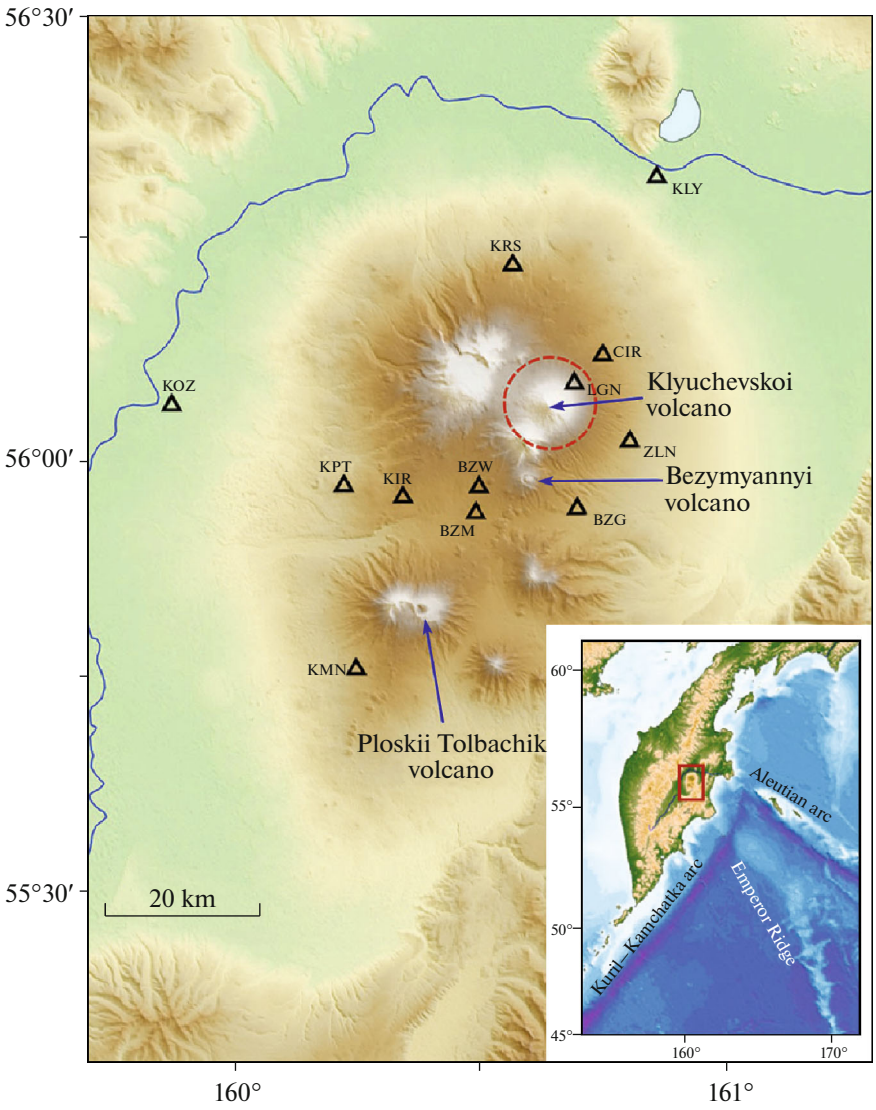


**Fig. 1.** Map of Klyuchevskoi volcanic group. Triangles show locations of KB GS RAS network stations. The main active volcanoes are indicated by arrows, red dotted line shows approximate position of cluster of DLP events ($h$ = 30–35 km).

and highly water-saturated crust of the Hawaiian–Emperor Ridge (Dorendorf et al., 2000), mantle flow around the edge of the Pacific Plate (Yogodzinski et al., 2001), or slab detachment from a subducting plate due to the recent structural rearrangement of the subduction beneath Kamchatka (Levin et al., 2002).

KVG volcanoes feature different eruption types ranging from the Hawaiian type effusive eruptions as those during the two recent Tolbachik eruptions to the catastrophic explosive eruptions, for example, the Bezymyannyi eruption in 1956. Numerous eruptions and other volcanic manifestations are accompanied by seismic activation (Ozerov et al., 2007; Ivanov, 2008; Senyukov et al., 2009; Senyukov, 2013; Droznin et al., 2015). A very interesting feature of KVG is the presence of one of the world's most active clusters of DLP earthquakes (Gorelchik and Storcheus, 2001; Gorelchik et al., 2004; Shapiro et al., 2017a). Previous studies have shown that the hypocenters of these earthquakes are localized within a small spatial domain beneath the Klyuchevskoi volcano at the crust–mantle boundary (at the depths of 30–35 km). In this work, we use the approximate position of the cluster of DLP events determined based on (Shapiro et al., 2017) (Fig. 1).

## DATA

Seismic monitoring at KVG is conducted by a network of permanent seismic stations of the Kamchatka Branch of the Geophysical Survey of the Russian Academy of Sciences (KB GS RAS) (Chebrov et al., 2013). The data from all seismic network stations are transferred to Petropavlovsk-Kamchatskii and uploaded to the servers of the regional information processing

center of the KB GS RAS in close-to-real-time mode. The data acquisition and transfer system is organized on the basis of the KB GS RAS local network using the Internet channels of two digital services providers (Rostelecom and InterKamService), RadioEthernet communication networks, OAO SetTelecom VSAT network, OAO Satis VSAT network based on "Idirect" technology with a hub in Petropavlovsk–Kamchatskii. The main file depot is a specialized seismic data archive servers based on two RAID 6 arrays. The data are stored in the form of daily files for each channel of each station (Chebrov, 2010, 2020).

In this work, we use radio telemetric seismic stations (RTSS) the signals from which are transmitted via radio channel with FM-FM modulation, directly or through a repeater, to the receiver centers in Kozyrevsk and Klyuchi villages where they are converted into digital records with a sampling frequency of 128 Hz. In this work, we used the records of the three-component CM3KV veloci meters with a frequency band of the recorded seismic signals of 0.7–20 Hz. The RTSS environment was developed in 1974–1982 for the purposes of on-line monitoring of active volcanoes (Gavrilov, 1987). The seismic stations used in this study are shown in Fig. 1.

## METHODS

### *Matched Filter Earthquake Detection Method*

Among the most common algorithms of automatic event detection, we selected the matched filter method (Van Trees, 1968) considering its main advantages: high sensitivity required for detecting weak LP earthquakes and relatively low computational costs. Thus, this algorithm searches for a priori known signal (waveform template) in the noisy time series by calculating the cross-correlation functions of the template signal with the successive segments of the incoming data stream. The fragments of the signal that have a high degree of similarity with the template waveform give a high value of the cross-correlation function. The detection sensitivity substantially increases in the case of simultaneous use of multicomponent seismic array records (Gibbons and Ringdal, 2006). In our study, the matched filter detection proves to be efficient due to a characteristic feature of the LP of earthquakes—the similarity of their waveforms (Shapiro et al., 2017a).

The first step in processing seismological data is bandpass filtering from 1 to 5 Hz and decimation. Figure 2 shows an hourly record (KMN station, *N*-component) containing several LP events. The template signal used for detection and the comparison of its waveform with the waveform of the selected earthquake are also displayed in this figure. The records of the template earthquake by all stations are presented in Fig. 3.

According to the selected algorithm, a window with a length of the template signal moves along the seismogram shifting at each step by one data count. Each time and at each component, the coefficient of correlation is calculated between the template and a signal segment of the same duration by the following formula:

$$CC(X,Y) = \frac{(X,Y)}{\|X\|\|Y\|}, \tag{2}$$

where $(X, Y)$ is the dot product of two vectors and $\|X\|$, $\|Y\|$ are their norms. If we represent vectors $X$, $Y$ in the form of the sets of the counts $x_i$, $y_i$, $i = 1, \ldots, n$ in time

$$X = \begin{pmatrix} x_1 \\ \ldots \\ x_n \end{pmatrix}, \quad Y = \begin{pmatrix} y_1 \\ \ldots \\ y_n \end{pmatrix}, \tag{3}$$

the dot product and the norms of these vectors are calculated by the following formula:

$$(X,Y) = \sum_{i=1}^{n} x_i y_i. \tag{4}$$

$$\|X\| = \sqrt{\sum_{i=1}^{n} x_i^2}, \quad \|Y\| = \sqrt{\sum_{i=1}^{n} y_i^2}. \tag{5}$$

For example, when applied to one component data, the algorithm yields a time series of the correlation coefficients for one day (Fig. 4a). In the case of the analysis of multicomponent records, the time series of the correlation coefficients for individual components are averaged. In this work, we used the records from ten stations of KB GS RAS seismic network. Thus, with the use of the described algorithm for seismogram processing, 30 time series of the correlation coefficients for each day of the studied period were averaged. The example illustrated in Fig. 4b shows that simultaneous analysis of multicomponent data results in a more to a more precise detection and makes the algorithm more selective.

As a result, the algorithm detects the signals whose quite complex waveforms including direct seismic waves and the code closely coincide with the initial template simultaneously in many components (including the correction for time delays between components). This waveform coincidence is only possible in the case when the sources of all the detected signals are located very close to each other (at least, not farther than within half a wavelength) and have almost identical mechanisms. Such a group of the earthquakes can be considered as highly probably being the result of the action of one source with very frequent recurrence.

The initial template used for detecting a group of the earthquakes generated by the same recurrent source (or by a group of identical and very closely

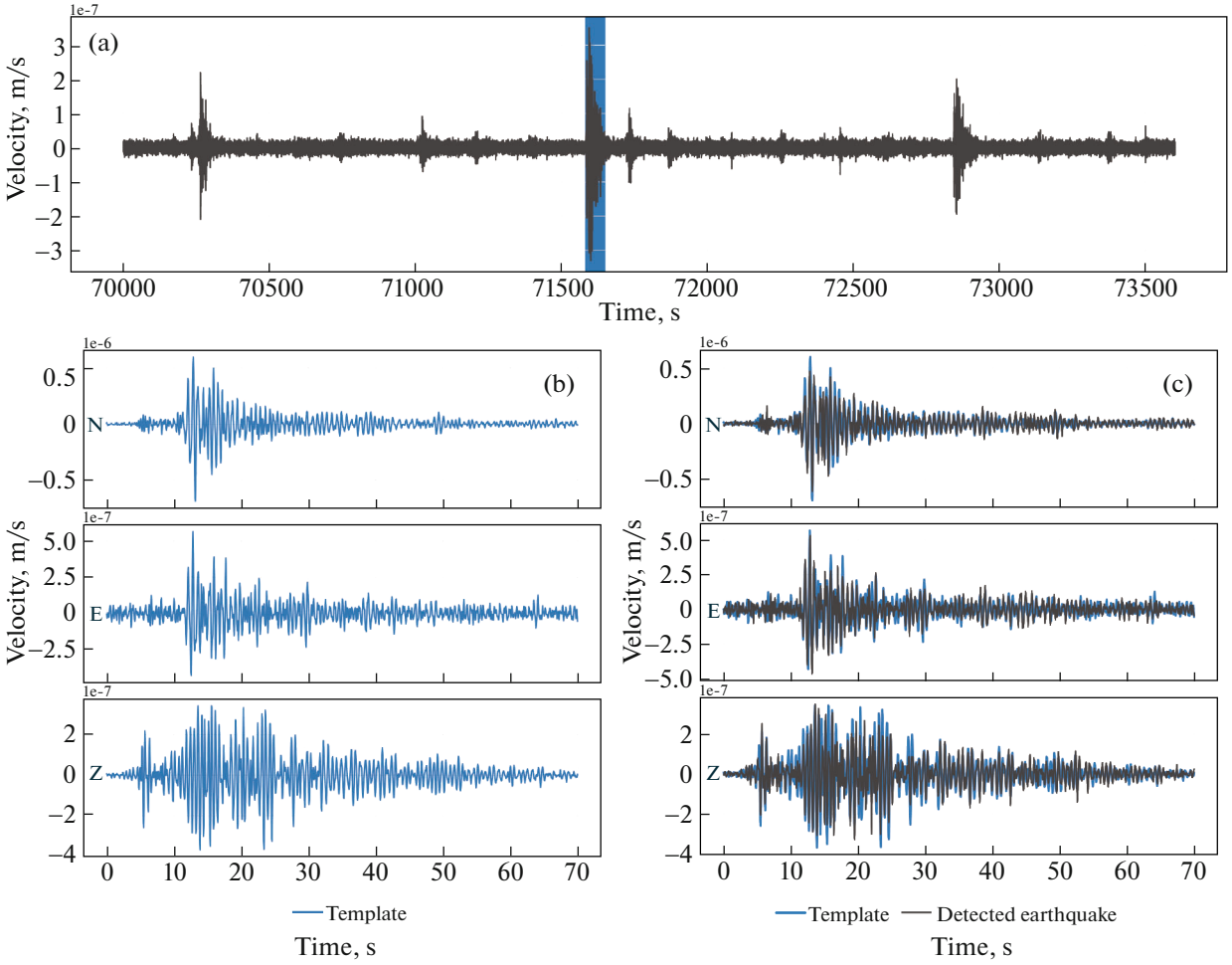


**Fig. 2.** Example of matched filter earthquake detection (all seismograms are band filtered from 1 to 5 Hz): (a) one hour of continuous seismic recording of *N*-component, KMN station; (b) template used for detection (June 26, 2012 12:26:10 PM), three components, KMN station; (c) example of detection at KMN station (event is shown in blue in panel (a)).

located sources) was selected, in a sense, at random. Therefore, for improving the detection quality, an averaged (stacked) template which is more representative of the entire group of the earthquakes is constructed. To this end, at the previous step, one should select all the detections which meet the condition $CC > 0.3$ and then average their waveforms. This averaging (stacking) reduces the contribution of the incoherent noise and constructively sums the correlated signals. Figure 5 shows the signals of the original and averaged templates for one component. After this, the procedure of calculation of the correlation coefficients is repeated with the averaged (stacked) template.

The detection criterion is that the averaged (mean) correlation coefficient over all stations exceeds a given threshold. At $CC_{\text{average}} < CC_{\text{threshold}}$, the detection is considered false and the corresponding *CC* value in the series is zeroed (Fig. 6). If the detection proves to be reliable, the moment magnitude of the detected event is calculated by the algorithm described in the Section below.

### *Determination of Earthquake Magnitudes*

Currently, it is common in Kamchatka to use the classification of the regional earthquakes in terms of their energy class *Ks* (Rautian, 1960; 1964) (the *S*-wave class determined from S.A. Fedotov's nomogram (Fedotov, 1972)). This quantitative characteristic was defined as

$$Ks = \log E, \tag{6}$$

where *E* is the energy (in joules) of seismic waves. The relationship between energy class and magnitude $m^{\text{CKM}}$ is described by the following formula (Gusev and Melnikova, 1990):

$$Ks = 2.00m^{\text{CKM}} + 1.68 \pm 0.55, \tag{7}$$

where $m^{\text{CKM}} \approx m_b + 0.18$, $m_b < 5.6$. The energy class *K* is determined from the nomogram constructed for the earthquakes of a given region based on the maximum ratio of the amplitude in the *S*-wave to its period $(A/T)_{\max}$ and the epicentral distance for the earth-

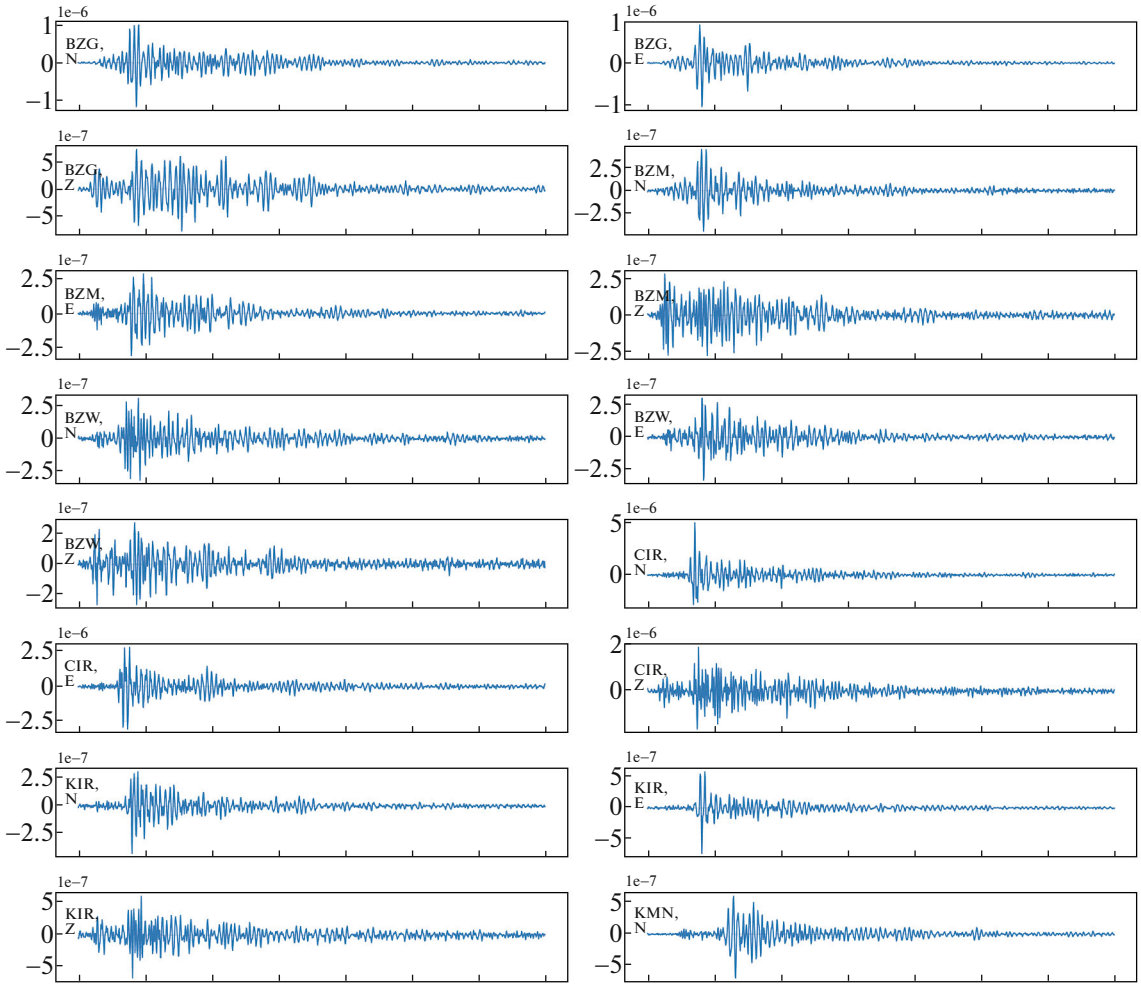


**Fig. 3.** Record of template earthquake at all stations (June 26, 2012, 12:26:10 PM).

quakes with a source depth $h = 0$–$200$ km. The nomogram was calibrated against the earthquakes with $K = 10$–$11$ which corresponds to the magnitudes 4.2–4.7. The magnitudes of the volcanic earthquakes are substantially lower which challenges the applicability of this magnitude determination method to the studied type of seismic events. Therefore, in this work, we use the classical definition of the moment magnitude (Kanamori, 1977; Hanks and Kanamori, 1979) with the calculation of the seismic moment. Despite the fact that the mechanism of the LP volcanic earthquakes highly likely differs from a pure shear along a fault (an idealized mechanism of tectonic earthquakes) and contains a significant volumetric component, it can be described by a seismic moment tensor (Wech et al., 2020) (in some cases, a superposition of this tensor and a force vector is considered) (Chouet and Matoza, 2013; Wech et al., 2020). In the case of tensor description of the source, it is possible to determine a scalar seismic moment. The latter will not necessarily be associated with the magnitude of the slip on the fault (as in the case of the tectonic earthquakes) but, rather, e.g., with a change in volume. For example, at the propagation of a magmatic melt through a system of microfaults, a probable geometry of a seismic source could be an opening crack. If so, the seismic moment tensor $M$ is written out as (Aki and Richards, 2002)

$$M = \begin{pmatrix} \lambda dV & 0 & 0 \\ 0 & \lambda dV & 0 \\ 0 & 0 & (\lambda + 2\mu) dV \end{pmatrix}, \quad (8)$$

where $\lambda$ and $\mu$ are the Lamé constants; $dV$ is the change in the volume of a crack. In the case of a Poisson medium ($\lambda = \mu$), the scalar seismic moment $M_0$ is $0.6\lambda dV$. The sources having this type of the mechanism emit more $S$-waves than $P$-waves (Shi and Ben-Zion, 2009), consistent with the observed signals of from DLP earthquakes (Shapiro et al., 2017; Wech et al., 2020). Based on these considerations, we propose to use the moment scale of magnitudes for the DLP earthquakes:

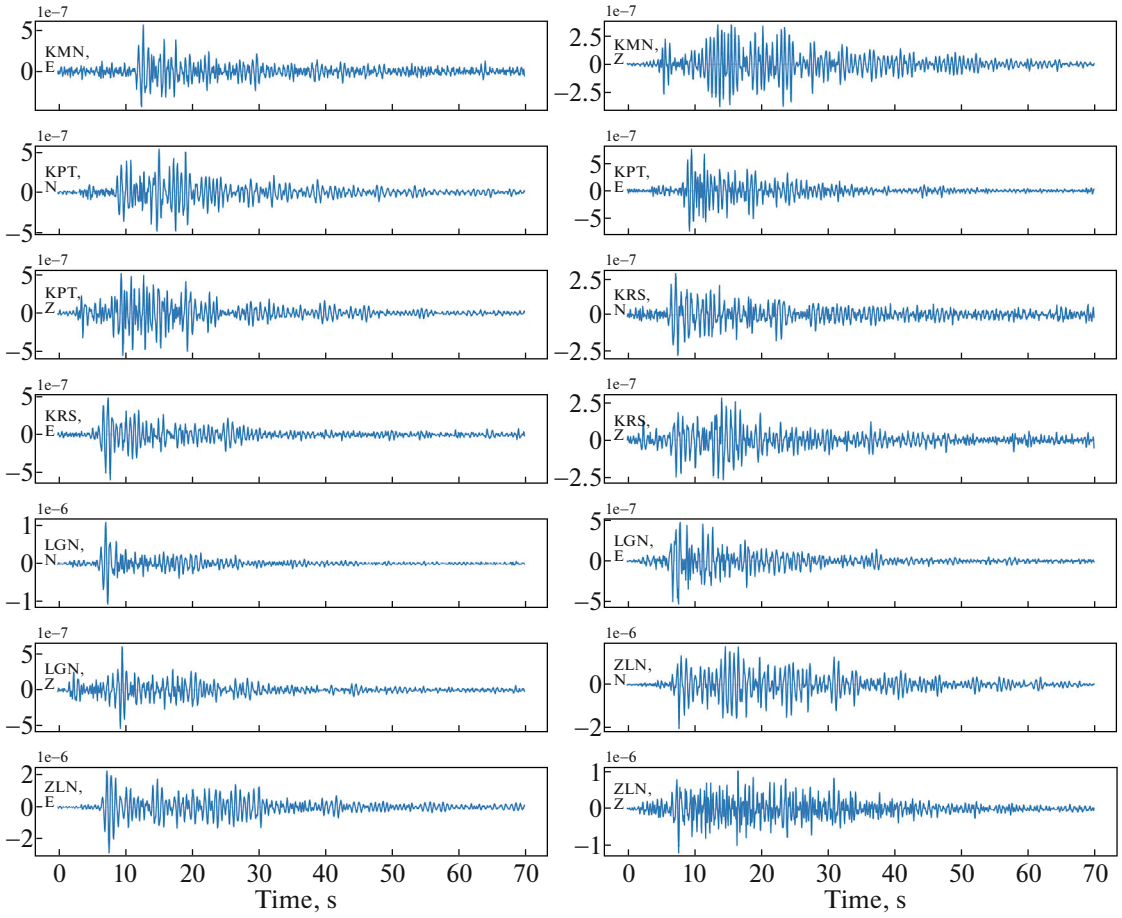


**Fig. 3.** (Contd.)

$$M_w = \frac{2}{3}(\log M_0 - 9.05). \quad (9)$$

The hypocenters of the studied DLP earthquakes are localized within a small spatial domain beneath the Klyuchevskoi volcano at the crust–mantle boundary (at the depths from 30 to 35 km) (Shapiro et al., 2017a). Thus, the distance from these hypocenters to the recording seismic stations is above ten wavelengths (for the frequencies on the order of 1.5 Hz used in this study). Therefore, the estimate of the seismic moment was obtained from the equations for ground surface displacements from *S*-waves in the far zone (Aki and Richards, 2002):

$$u(\mathbf{x},t) = \gamma \frac{\dot{M}_0(t - r/\beta)}{4\pi\rho\beta^3 r}, \quad (10)$$

where $M_0$ is the seismic moment; $t$ is time; $\beta$ is the *S*-wave velocity; $\rho$ is density of the medium; $r$ is the distance from the hypocenter to the observation point $x$; $\gamma$ is a factor associated with the radiation pattern of the source. In the practical calculations of magnitudes, the full seismic moment tensor and the corresponding radiation pattern are not estimated (largely due to the complexity and instability of the estimation procedure). Instead, it is assumed that the use of the records from multiple stations and components averages this factor. Therefore, in the subsequent analysis, we use the approximate value $\gamma = 1$. Thus, from formula (10) it follows:

$$\dot{M}_0 \sim 4\pi\rho\beta^3 r u^S. \quad (11)$$

Calculating the derivative of the displacement in the Fourier domain, we obtain:

$$v^S \sim \dot{u}^S \sim 2\pi f u^S, \quad (12)$$

where $u^S$ and $v^S$ are the amplitudes of the displacement and velocity records, respectively; $f$ is the characteristic signal frequency for *S*-waves. The final estimate of the seismic moment is

$$M_0 \sim \frac{4\pi\rho\beta^3 r u^S}{2\pi f} = \frac{\rho\beta^3 r}{\pi f^2}\left|v^S_{\max}\right|, \quad (13)$$

where $\left|v^S_{\max}\right|$ is the maximum amplitude in the record of the earthquake. The distances $r$ are calculated from the known depth ($h$ = 32 km) of the magma reservoir

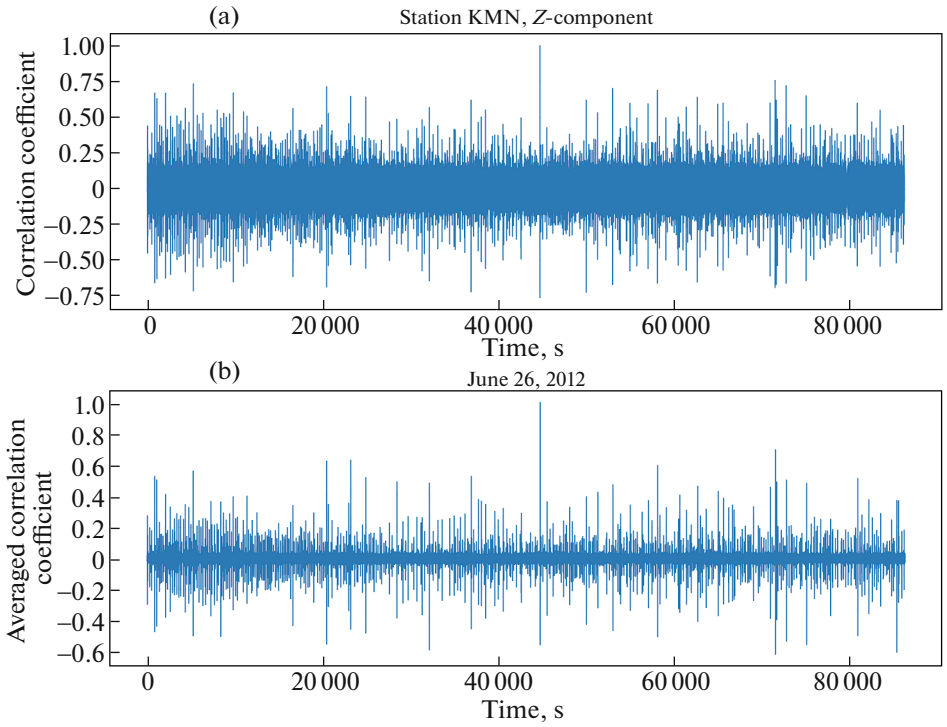


**Fig. 4.** Time series of correlation coefficients for one day of records. Single peak with $CC = 1$ corresponds to the record segment containing the template signal (June 26, 2012, 12:26:10 PM): (a) result for the vertical component at KMN station; (b) correlation coefficient averaged over all the ten stations and tree components.

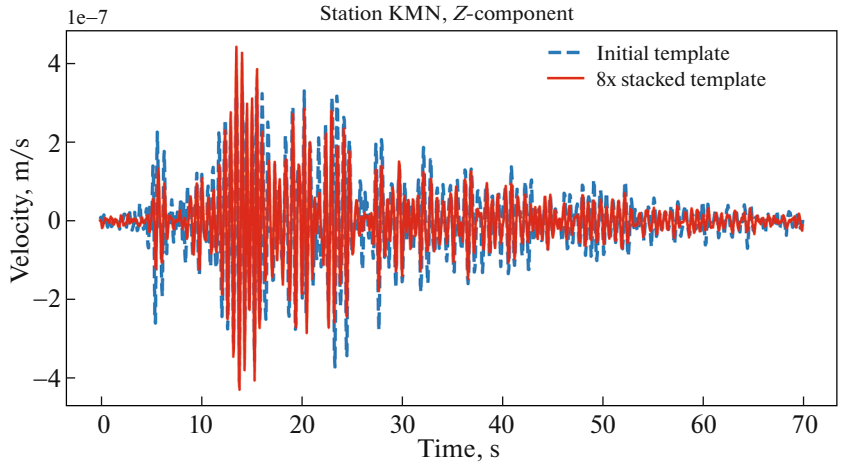


**Fig. 5.** Blue dashed line is initial template, red solid line is averaged template with amplitude increased by a factor of 8.

and the coordinates of seismic stations. In our calculations, we assumed the following parameters of the medium: $\rho = 3000$ kg/m$^3$, $\beta = 3500$ m/s.

Based on the results of visual inspection of the amplitude Fourier spectra at different stations and components (example in Fig. 7), we decided to use the value of the characteristic frequency $f = 1.5$ Hz.

The maximum displacement velocities at an individual station were calculated from three components:

$$\overline{\left|V^S_{\max}\right|} = \sqrt{\sum_{j=1}^{3} V^2_{j_{\max}}}, \tag{14}$$

where $V_{j_{\max}}$ is the maximum displacement velocity in the $j$th component of the station. From the obtained $\left|V^S_{\max}\right|$, the seismic moments (13) and moment magnitudes (8) are calculated at each station, and the obtained values are then averaged over all stations:

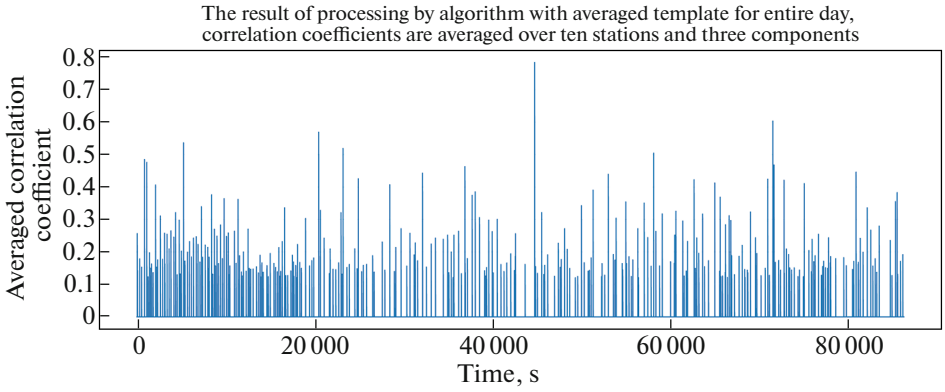


**Fig. 6.** Result of detection with the stacked template over all stations and components $CC_{average} < CC_{threshold}$ (in this case, threshold value of correlation coefficient is 0.12).

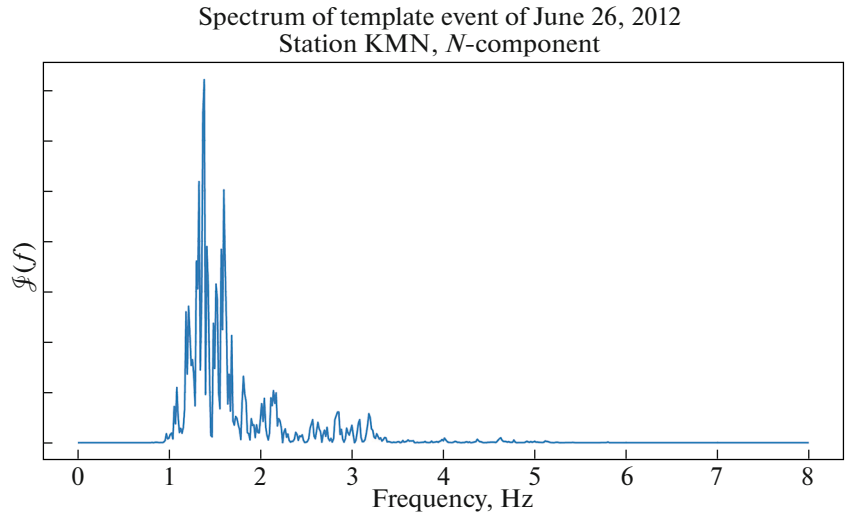


**Fig 7.** Example of amplitude Fourier spectrum from DLP earthquake (station KMN, *N*-component; template is shown in Fig. 2).

$$\bar{M}_w = \frac{1}{N}\sum_{i=1}^{N} M_w^i. \quad (15)$$

## DISCUSSION AND CONCLUSIONS

We have processed the seismograms obtained by the KB GS RAS network stations from January 1, 2011 to December 31, 2012 using more than 400 template earthquakes selected from the KB GS RAS catalog of volcanic earthquakes (Senyukov et al., 2013; 2014). The result of the processing for each template is earthquake subcatalog in which each seismic event has in correspondence the value of the coefficient of correlation between its signal and the template used in its processing as well as the value of the moment magnitude. The minimum threshold value of the correlation coefficient for including an earthquake is the catalog is $CC_{min} = 0.08$. For each $CC_i$ value, starting from $CC_{min}$ with a step of 0.02, we compiled a set of the earthquakes whose correlation coefficients were higher than $CC_i$. Based on the results of the performed statistical analysis, for the subsequent study we decided to use the samples composed of the seismic events with $CC = 0.12$. As a result, for the period 2011–2012, we obtained a catalog of 48915 earthquakes with the use of all templates.

In Fig. 8, we analyze the recurrence of the earthquakes from one of the largest subcatalogs obtained with the initial template which is shown in Figs. 2, 3, 5, 7 and includes 11627 events. We consider the probable ways to approximate the obtained frequency–magnitude graph. It is logical to begin with the power-law testing (Fig. 8b); however, the b-value of the resulting linear relationship proves to be overestimated ($b = 3.4$), consistent with the results obtained from the catalogs of the volcanic earthquakes in several previous works, e.g., (Senyukov, 2013). The *b*-value was estimated by the least square technique in the interval of magnitudes starting from $M_w = 1.40$. In this case, we do not intend to find the best approximation of the frequency–magnitude dependence but, rather, show

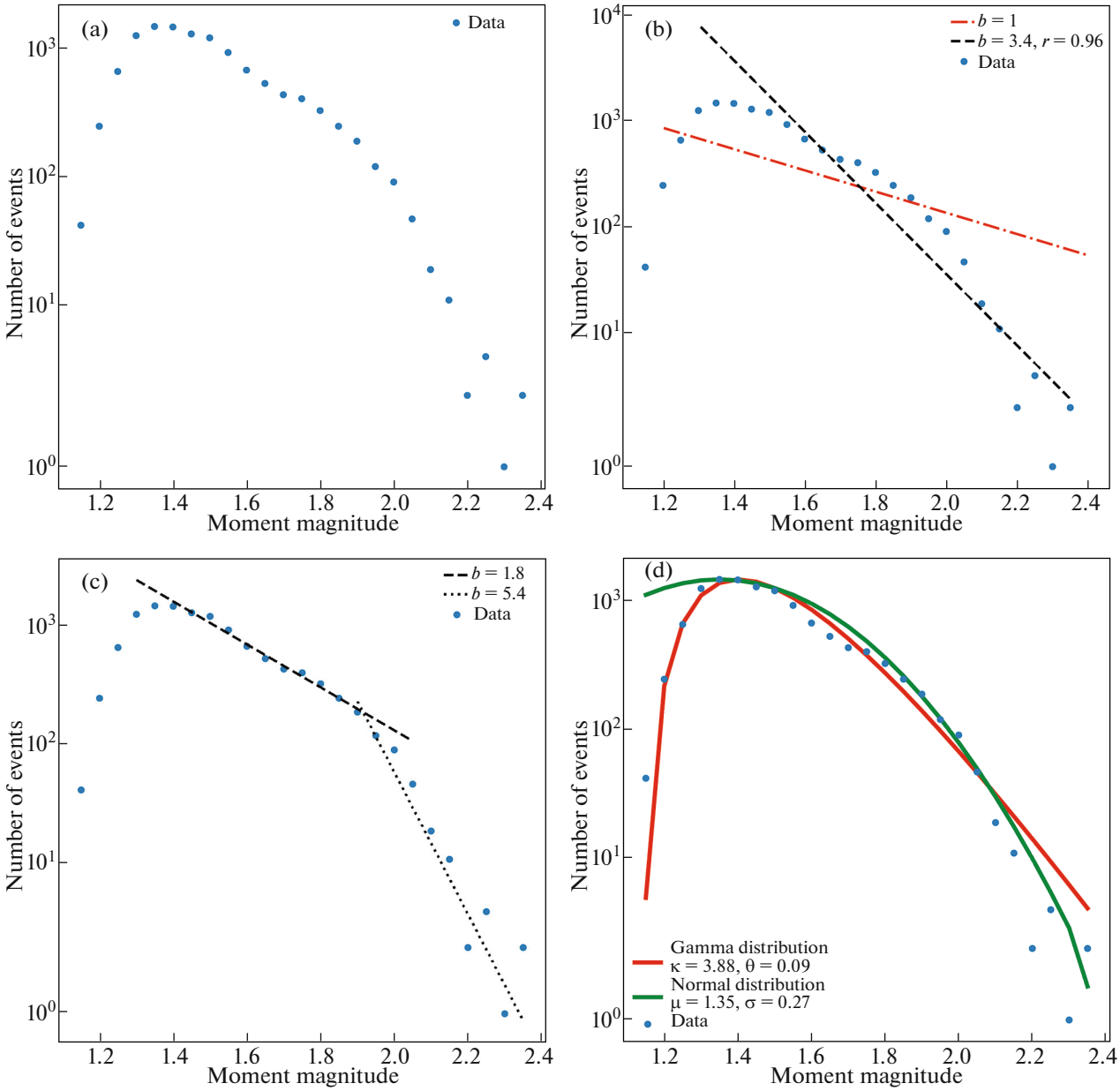


**Fig. 8.** Graph of frequency–magnitude distribution for subcatalog obtained based on template shown in Figs. 2, 3, 5, and 7: (a) results of observation processing; (b) possible approximation with Gutenberg–Richter law; (c) possible approximation with two Gutenberg–Richter laws; (d) possible approximation with distributions with characteristic magnitude value.

that the $b$-value is in any case strongly above 1 (a line with the corresponding slope is drawn on the graph). The graph has a break which divides the distribution into two parts, each of which can also be approximated by the straight lines with different slopes ($b_1 = 1.8$ for $M_w = 1.40–1.90$ and $b_2 = 5.4$ for $M_w = 1.90–2.35$, Fig. 8c). Vorobieva et al. (2016) associate these breaks with the lack of the strong earthquakes: a rapid creep reduces the probability of a large seismic rupture to emerge. However, this theory was developed for the tectonic earthquakes and, hence, it is barely applicable for the studied LP events. The authors of (Okada et al., 1981; Main, 1987; Lahr et al., 1994) note that the frequency–magnitude graphs of the volcanic earthquakes obviously deviate from the Gutenberg–Richter distribution.

The frequency–magnitude graph obtained in this study can also be described by the distributions other than power-law (Fig. 8d), for instance, by the normal distribution:

$$f_X(x) = \frac{1}{\sigma\sqrt{2\pi}} e^{-\frac{(x-\mu)^2}{2\sigma^2}} \quad (16)$$

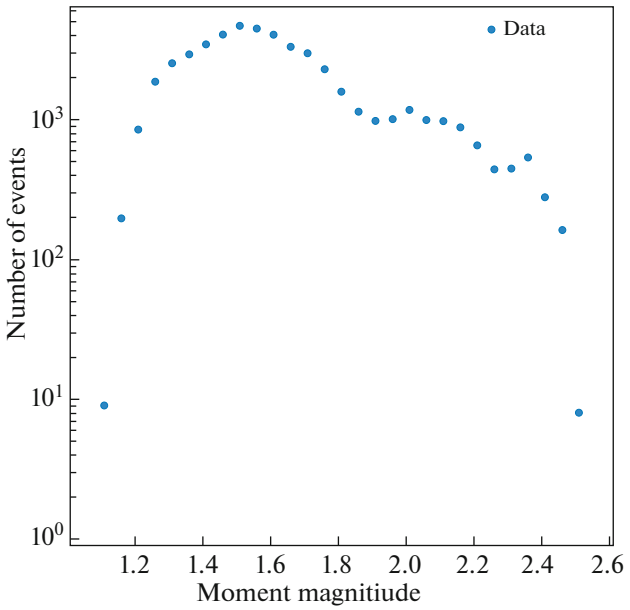


**Fig. 9.** Frequency–magnitude graph for complete catalog of DLP earthquakes obtained in this work.

with the standard deviation $\sigma = 0.27$ and the mean $\mu = 1.35$. The gamma distribution

$$f_X(x) = \begin{cases} x^{k-1}\dfrac{e^{-x/\theta}}{\theta^k \Gamma(k)}, & x \geq 0 \\ 0, & x < 0 \end{cases} \quad (17)$$

with parameters $\theta = 0.09$ and $k = 3.88$, where $\Gamma(k)$ is the Euler function, is another probable model.

From Fig. 8d it can be seen that the left branch of the observed frequency–magnitude graph is more accurately approximated by the gamma distribution, whereas a better fit for the right branch is provided by the normal distribution. From the general considerations, it is barely plausible that a physical process responsible for seismicity associated with a magma source can be described by a combination of two distributions. Thus, for the subsequent statistical generalizations, we must decide in favor of some either one of the distributions. At this stage of the study, we prefer the normal distribution considering the following arguments: (1) it has a higher level of significance in the approximation of the right branch of the observed frequency–magnitude graph; (2) there are reasonable doubts about the completeness of the sample of the low-magnitude earthquakes (left branch) because of the o insufficient sensitivity of the network (or the effects of network blinding due to volcanic tremors); (3) the weak physical validity of the application of the gamma distribution, whereas in the case of a homogeneous source, there is grounds to expect a normal distribution of the parameters of seismic events.

The distributions obtained for the group of the similar DLP earthquakes beneath the Klyuchevskoi volcano substantially differ from the Gutenberg–Richter relationship by the fact that for these earthquakes it is possible to determine a scale parameter that corresponds to a certain characteristic source size. This characteristic size scaling is fairly consistent with the generation of numerous recurrent earthquakes by a single source. The existence of these sources is described by the models considering pressure variations in magma. Seismic waves in these models can either be generated by a periodic pressure drop through mechanical barriers/valves (Shapiro et al., 2018; Wech et al., 2020) or by rapid avalanche-like degassing leading to a growth in pressure (Melnik et al., 2020). We note that for this type of the earthquakes, the "standard" analysis of the frequency–magnitude relationship with estimation of the *b*-value is meaningless as the obtained values will vary depending on the used magnitude range.

In Fig. 9, we present the frequency–magnitude graph for the complete catalog of DLP earthquakes beneath the Klyuchevskoi volcano, which combines the subcatalogs obtained based on all the selected templates. The resulting distribution has a complex shape with several local maxima. We interpret this effect as the result of overlapping of the distributions from the sources with several characteristic sizes.

## ACKNOWLEDGMENTS

We are grateful to Geneviève Moguilny for her help in conducting calculations at the IPGP Parallel Computing and Data Analysis Platform for Earth Science (S-CAPAD), France.

## FUNDING

The work was supported by the Ministry of Science and Education of the Russian Federation under the project no. 14.W03.31.0033 "Geophysical research, monitoring and forecast of the development of catastrophic geodynamic processes in the Far East of the Russian Federation" and by the European Research Council (ERC) under the project no. 787399-SEISMAZE.

The research by KB GS RAS employees was also carried out under the research and development project no. AAAA-A19-119031590060-3 "Integrated geophysical studies of volcanoes in Kamchatka and northern Kuril Islands aimed at detecting the signs of impending eruption and predict its dynamics with the assessment of ash hazard for aviation."

## REFERENCES

Aki, K. and Koyanagi, R., Deep volcanic tremor and magma ascent mechanism under Kilauea, Hawaii, *J. Geophys. Res.: Solid Earth*, 1981, vol. 86, no. B8, pp. 7095–7109.

Aki, K. and Richards, P.G., *Quantitative Seismology*, 2nd ed., Sausalito, USA: Univ. Sci. Books, 2002.

Aso, N. and Tsai, V.C., Cooling magma model for deep volcanic long-period earthquakes, *J. Geophys. Res.*, 2014, vol. 119, pp. 8442–8456.

Aso, N., Ohta, K., and Ide, S., Tectonic, volcanic, and semi-volcanic deep low-frequency earthquakes in western Japan, *Tectonophysics*, 2013, vol. 600, pp. 27–40.

Bean, C.J., de Barros, L., Lokmer, I., Métaxian, J.P., O'Brien, G., and Murphy, S., Long-period seismicity in the shallow volcanic edifice formed from slow-rupture earthquakes, *Nat. Geosci.*, 2014, vol. 7, pp. 71–75.

Chebrov, D.V., Droznina, S.Ya., Senyukov, S.L., Shevchenko, Yu.V., and Mityushkina, S.V., Chebrov, V.N., Droznin, D.V., Sergeev, V.A., and Pantyukhin, E.A., A system for acquisition, processing, storing and representing seismological data and the results of their processing in the SP SPTs, hardware, algorithms and software, in *Problemy kompleksnogo geofizicheskogo monitoringa Dal'nego Vostoka Rossii: Tr. vtoroi reg. nauchno-tekh. konf.* (Problems of Integrated Geophysical Monitoring of the Russian Far East: Proc. 2nd Reg. Sci. Tech. Conf.), Chebrov, V.N., Ed., Petropavlovsk-Kamchatskii: GS RAN, 2010, pp. 332–336.

Chebrov, V.N., Droznin, D.V., Kugaenko, Yu.A., Levina, V.I., Senyukov, S.L., Sergeev, V.A., Shevchenko, Yu.V., and Yashchuk, V.V., The system of detailed seismological observations in Kamchatka in 2011, *J. Volcanol. Seismol.*, 2013, vol. 7, no. 1, pp. 16–36.

Kamchatka and the Commander Islands, in *Ezheg. "Zemletryaseniya Rossii v 2018 godu"* (Yearbook "Earthquakes of Russia in 2018"), Malovichko, A.A., Ed., Obninsk: FITS EGS RAN, 2020, pp. 71–81.

Chouet, B.A., Long-period volcano seismicity: its source and use in eruption forecasting, *Nature*, 1996, vol. 380, no. 6572, pp. 309–316.

Chouet, B.A. and Matoza, R.S., A multi-decadal view of seismic methods for detecting precursors of magma movement and eruption, *J. Volcanol. Geotherm. Res.*, 2013, vol. 252, pp. 108–175.

Dorendorf, F., Wiechert, U., and Wörner, G., Hydrated sub-arc mantle: a source for the Kluchevskoy volcano, Kamchatka/Russia, *Earth Planet. Sci. Lett.*, 2000, vol. 175, nos. 1–2, pp. 69–86.

Droznin, D.V., Shapiro, N.M., Droznina, S.Ya., Senyukov, S.L., Chebrov, V.N., and Gordeev, E.I., Detecting and locating volcanic tremors on the Klyuchevskoi group of volcanoes (Kamchatka) based on correlations of continuous seismic records, *Geophys. J. Int.*, 2015, vol. 203, no. 2, pp. 1001–1010.

Fedotov, S.A., *Energeticheskaya klassifikatsiya Kurilo-Kamchatskikh zemletryasenii i problema magnitud* (Energy Classification of Kuril-Kamchatka Earthquakes and the Magnitude Problem), Moscow: Nauka, 1972.

Gavrilov, V.A., Voropaev, V.F., Golovshchikova, I.A., et al., System of radio telemetry instrumentss TESI_2, *Seism. Prib.*, 1987, vol. 19, pp. 5–16.

Gibbons, S.J. and Ringdal, F., The detection of low magnitude seismic events using array-based waveform correlation, *Geophys. J. Int.*, 2006, vol. 165, no. 1, pp. 149–166.

Gordeev, E.I., Seismicity of volcanoes and monitoring of volcanic activity, *Vestn. DVO Ross. Akad. Nauk*, 2007, vol. 132, no. 2, pp. 38–45.

Gorelchik, V.I. and Storcheus, A.V., Deep long-period earthquakes beneath the Klyuchevskoi volcano, Kamchatka, in *Geodinamika i vulkanizm Kurilo-Kamchatskoi ostrovoduzhnoi sistemy* (Geodynamics and Volcanism of the Kuril-Kamchatka Island Arc System), Ivanov, B.V., Ed., Petropavlovsk-Kamchatskii: IVGiG DVO RAN, 2001, pp. 373–389.

Gorelchik, V.I., Garbuzova, V.T., and Storcheus, A.V., Deep-seated volcanic processes beneath Klyuchevskoi volcano as inferred from seismological data, *J. Volcanol. Seismol.*, 2004, vol. 6, pp. 21–34.

Gusev, A.A. and Melnikova, V.N., Relations between magnitudes: global and Kamchatka data, *Volcanol. Seismol.*, 1990, vol. 6, pp. 55–63.

Gutenberg, B. and Richter, C.F., Frequency of earthquakes in California, *Bull. Seismol. Soc. Am.*, 1944, vol. 34, no. 4, pp. 185–188.

Hanks, T.C. and Kanamori, H., A moment magnitude scale, *J. Geophys. Res.*, 1979, vol. 84, no. 5, pp. 2348–2350.

Hensch, M., Dahm, T., Ritter, J., Heimann, S., Schmidt, B., Stange, S., and Lehmann, K., Deep low-frequency earthquakes reveal ongoing magmatic recharge beneath Laacher See Volcano (Eifel, Germany), *Geophys. J. Int.*, 2019, vol. 216, no. 3, pp. 2025–2036.

Ivanov, V.V., Current cycle of the Kluchevskoi volcano activity in 1995–2008 based on seismological, photo, video and visual data, *Proc. of Conf. Devoted to Volcanologist Day*, Petropavlovsk-Kamchatskii, 2008, pp. 100–109.

Iverson, R.M., Dzurisin, D., Gardner, C.A., Gerlach, T.M., LaHusen, R.G., Lisowski, M., Major, J.J., Malone, S.D., Messerich, J.A., Moran, S.C., Pallister, J.S., Qamar, A.I., Schilling, S.P., and Vallance, J.W., Dynamics of seismogenic volcanic extrusion at Mount St. Helens in 2004–05, *Nature*, 2006, vol. 444, pp. 439–443.

Kanamori, H., The energy release in great earthquakes, *J. Geophys. Res.*, 1977, vol. 82, no. 20, pp. 2981–2987.

Kanamori, H. and Anderson, D.L., Theoretical basis of some empirical relations in seismology, *Bull. Seismol. Soc. Am.*, 1975, vol. 65, no. 5, pp. 1073–1095.

Kurihara, R., Obara, K., Takeo, A., and Tanaka, Y., Deep low-frequency earthquakes associated with the eruptions of Shinmoe-dake in Kirishima volcanoes, *J. Geophys. Res.: Solid Earth*, 2019, vol. 124, no. 12, pp. 13079–13095.

Lahr, J.C., Chouet, B.A., Stephens, C.D., Power, J.A., and Page R.A. Earthquake classification, location, and error analysis in a volcanic environment: implications for the magmatic system of the 1989–1990 eruptions at redoubt volcano, Alaska, *J. Volcanol. Geotherm. Res.*, 1994, vol. 62, nos. 1–4, pp. 137–151.

Levin, V., Shapiro, N.M., Park, J., and Ritzwoller, M. H., Seismic evidence for catastrophic slab loss beneath Kamchatka, *Nature*, 2002, vol. 418, no. 6899, pp. 763–767.

Main, I.G., A characteristic earthquake model of the seismicity preceding the eruption of Mount St. Helens on 18 May 1980, *Phys. Earth Planet. Inter.*, 1987, vol. 49, nos. 3–4, pp. 283–293.

Melnik, O., Lyakhovsky, V., Shapiro, N.M., Galina, N., and Bergal-Kuvikas, O., Deep long period volcanic earthquakes generated by degassing of volatile-rich basaltic magmas, *Nat. Commun.*, 2020, vol. 11, Article number 3918. https://doi.org/10.1038/s41467-020-17759-4

Neuberg, J.W., Tuffen, H., Collier, L., Green, D., Powell, T., and Dingwell, D., The trigger mechanism of low-frequency

earthquakes on Montserrat, *J. Volcanol. Geotherm. Res.*, 2006, vol. 153, nos. 1–2, pp. 37–50.

Nichols, M.L., Malone, S.D., Moran, S.C., Thelen, W.A., and Vidale, J.E., Deep long-period earthquakes beneath Washington and Oregon volcanoes, *J. Volcanol. Geotherm. Res.*, 2011, vol. 200, nos. 3–4, pp. 116–128.

Okada, H., Watanabe, H., Yamashita, H., and Yokoyama, I., Seismological significance of the 1977–1978 eruptions and the magma intrusion process of Usu volcano, Hokkaido, *J. Volcanol. Geotherm. Res.*, 1981, vol. 9, no. 4, pp. 311–334.

Ozerov, A.Yu., Firstov, P.P., and Gavrilov, V.A., Periodicities in the dynamics of eruptions of Klyuchevskoi volcano, Kamchatka, in *Geophysical Monograph Series: Volcanism and Subduction "The Kamchatka Region,"* Eichelberger, J., Gordeev, E., Izbekov, P., Kasahara, M., and Lees, J., Eds., Washington: Am. Geophys. Union, vol. 172, pp. 283–291.

Power, J.A., Stihler, S.D., White, R.A., and Moran, S.C., Observations of deep long-period (DLP) seismic events beneath Aleutian arc volcanoes; 1989–2002, *J. Volcanol. Geotherm. Res.*, 2004, vol. 138, nos. 3–4, pp. 243–266.

Rautian, T.G., Energy of earthquakes, in *Metody detal'nogo izucheniya seismichnosti: Tr. IFZ AN SSSR, tom 176, nom. 9* (Methods for a Detailed Study of Seismicity, vol. 176, no. 9 of Proc. Inst. Phys. Earth Acad. Sci. USSR), Riznichenko, Yu.V., Ed., Moscow: IFZ AN SSSR, 1960, pp. 75–114.

Rautian, T.G., On the determination of the energy of earthquakes at a distance of up to 3000 km, in *Eksperimental'naya seismika: Tr. IFZ AN SSSR, tom 199, nom. 32* (Experimental Seismics, vol. 199, no. 32 of Proc. Inst. Phys. Earth Acad. Sci. USSR), Sadovskii, M.A., Ed., Moscow: Nauka, 1964, pp. 88–93.

Roman, D.C. and Cashman, K.V., The origin of volcano-tectonic earthquake swarms, *Geology*, 2006, vol. 34, no. 6, pp. 457–460.

Senyukov, S.L., Monitoring and prediction of volcanic activity in Kamchatka from seismological data: 2000–2010, *J. Volcanol. Seismol.*, 2013, vol. 7, no. 1, pp. 86–97.

Senyukov, S.L., *Prognoz izverzhenii vulkanov Klyuchevskoi i Bezymyannyi na Kamchatke* (Forecast of the Eruptions of the Klyuchevskoi and Bezymyannyi Volcanoes in Kamchatka), Saarbrücken: LAP Lambert Acad. Publishing, 2013.

Senyukov, S.L., Droznina, S.Ya., Nuzhdina, I.N., Garbuzova, V.T., and Kozhevnikova, T.Y., Studies in the activity of Klyuchevskoi volcano by remote sensing techniques between January 1, 2001 and July 31, 2005, *J. Volcanol. Seismol.*, 2009, vol. 3, no. 3, pp. 191–199.

Senyukov, S.L., Nuzhdina, I.N., and Chebrov, V. N., Seismic monitoring of volcanic regions of Kamchatka, in *Ezheg. "Zemletryaseniya Rossii v 2011 godu"* (Yearbook "Earthquakes of Russia in 2011"), Malovichko, A.A., Ed., Obninsk: GC RAN, 2013, pp. 75–79.

Senyukov, S.L., Nuzhdina, I.N., and Chebrov, V. N., Seismic monitoring of volcanic regions of Kamchatka, in *Ezheg. "Zemletryaseniya Rossii v 2012 godu"* (Yearbook "Earthquakes of Russia in 2012"), Malovichko, A.A., Ed., Obninsk: GC RAN, 2014, pp. 77–81.

Shapiro, N.M., Droznin, D.V., Droznina, S.Ya., Senyukov, S.L., Gusev, A.A., and Gordeev, E.I., Deep and shallow long-period volcanic seismicity linked by fluid-pressure transfer, *Nat. Geosci.*, 2017a, vol. 10, no. 6, p. 442–445.

Shapiro, N.M., Sens-Schönfelder, C., Lühr, B.G., Weber, M., Abkadyrov, I., Gordeev, E.I., Koulakov, I., Jakovlev, A., Kugaenko, Y.A, and Saltykov, V.A., Understanding Kamchatka's extraordinary volcano cluster, *Eos, Trans. Am. Geophys. Union*, 2017b, vol. 98, no. 7, pp. 12–17.

Shapiro, N.M., Campillo, M., Kaminski, E., Vilotte, J.-P., and Jaupart, C., Low-frequency earthquakes and pore pressure transients in subduction zones, *Geophys. Res. Lett.*, 2018, vol. 45, no. 20, pp. 11083–11094.

Shaw, B.E., Constant stress drop from small to great earthquakes in magnitude-area scaling, *Bull. Seismol. Soc. Am.*, 2009, vol. 99, no. 2A, pp. 871–875.

Shaw, H.R. and Chouet, B.A., Singularity spectrum of intermittent seismic tremor at Kilauea volcano, Hawaii, *Geophys. Res. Lett.*, 1989, vol. 16, no. 2, pp. 195–198.

Shi, Z. and Ben-Zion, Y., Seismic radiation from tensile and shear point dislocations between similar and dissimilar solids, *Geophys. J. Int.*, 2009, vol. 179, no. 1, pp. 444–458.

Stein, S. and Wysession, M., *An Introduction to Seismology, Earthquakes, and Earth Structure*, Oxford: Blackwell Publ., 2003.

Tokarev, P.I., *Vulkanicheskie zemletryaseniya Kamchatki* (Volcanic Earthquakes in Kamchatka), Moscow: Nauka, 1981.

van Tees, H.L., *Detection, Estimation and Modulation Theory, Part I: Detection, Estimation, and Linear Modulation Theory,* New York: Wiley, 1968.

Vorobieva, I., Shebalin, P., and Narteau, C., Break of slope in earthquake size distribution and creep rate along the San Andreas fault system, *Geophys. Res. Lett.*, 2016, vol. 43, no. 13, pp. 6869–6875.

Wech, A.G., Thelen, W.A., and Thomas, A.M., Deep long-period earthquakes generated by second boiling beneath Mauna Kea volcano, *Science*, 2020, vol. 368, no. 6492, pp. 775–779.

White, R., Precursory deep long-period earthquakes at Mount Pinatubo: Spatio-temporal link to a basalt trigger?, in *Fire and Mud: Eruptions and Lahars of Mount Pinatubo, Philippines*, Newhall, C.G. and Punongbayan, R.S., Eds., Seattle: Univ. Washington Press, 1996, pp. 307–327.

Yogodzinski, G.M., Lees, J.M., Churikova, T.G., Dorendorf, F., Wöerner, G., and Volynets, O.N., Geochemical evidence for the melting of subducting oceanic lithosphere at plate edges, *Nature*, 2001, vol. 409, no. 6819, pp. 500–504.

*Translated by M. Nazarenko*